Fabrication and VUV luminescence of $Lu_2O_3:Eu^{3+}$ (5 at.%) nanopowders and transparent ceramics

N.A. Safronova[1,*], R.P. Yavetskiy[1], O.S. Kryzhanovska[1], S.V. Parkhomenko[1], A.G. Doroshenko[1], M.V. Dobrotvorska[1], A.V. Tolmachev[1], R. Boulesteix[2], A. Maître[2],T. Zorenko[3,4], Yu. Zorenko[3,4]

[1]*Institute for Single Crystals, NAS of Ukraine, 60 Nauky Ave., Kharkiv, Ukraine 61072*

[2]*Univ. Limoges, IRCER, UMR CNRS 7315, 12 rue Atlantis, Limoges, France*

[3]*ElectronicDepartmentIvanFrankoUniversity in Lviv, Gen. Tarnavski str., 107, 79036, Lviv, Ukraine*

[4]*Institute of Physics, Kazimierz Wielki University in Bydgoszcz, 85-090 Bydgoszcz, Poland*

Abstract

Low-agglomerated $Lu_2O_3:Eu^{3+}$ 5 at.% nanopowders, as well as transparent ceramics were fabricated by co-precipitation with ammonium hydrogen carbonate and vacuum sintering method, respectively. It was determined that transition of a part of europium ions into the divalent state enhanced sinterability due to formation of anionic vacancies and decrease the covalency of RE-O bonds. The luminescent properties of the $Lu_2O_3:Eu^{3+}$ 5 at.% nanopowders and ceramics were studied under excitation by synchrotron radiation. The difference in the excitation spectra of $Lu_2O_3:Eu^{3+}$nanopowders and ceramics are caused by participation of the F^+ centers in the excitation processes of Eu^{3+} luminescence in Lu_2O_3 host. Finally, the locations of the energy levels related to the Eu^{3+} dopant in Lu_2O_3 matrix were determined.

Keywords:$Lu_2O_3:Eu^{3+}$nanopowders; Vacuum sintering; Transparent ceramics; Luminescent properties; VUV spectroscopy;Energy level diagram.

*Corresponding author. Tel.: +38(057) 3410277; fax: +38(057) 3409343.
E-mail address: nadiandu@gmail.com, (N.A. Safronova)
Institute for Single Crystals, NAS of Ukraine
60 Nauky Ave., Kharkiv, 61072, Ukraine

1 Introduction

The processes of relaxation of electronic excitationsin wide-gap dielectrics have been studied for many decades. The greatest successes have been achieved for simple binary oxides with a predominantly ionic bond type (MgO, BeO). In complex oxides (including sesquioxides) there is a large number of ways of forming structural and chemical bonds between atoms. To describe the dynamics of electron excitations in complex oxides, a simple relaxation model based on the consideration of the lower states of the electron-hole continuum and the assumption of the presence of several channels of relaxation of electron excitations is used [1]. The significant heterogeneity (including spatial) of the electronic structure of oxide compounds causes a branching of the relaxation channels. Theoxygen ions forming the valence band states are located in low-symmetric crystallographic positions, what leads to heterogeneities of the electronic structure. Narrow sub-bands near the valence band's top are formed by the non-bridging p-type oxygen orbitals, whereas in the depths the valence band has a structure typical for the traditional ionic (covalent) crystals [2]. Transitions involving states of different sub-bands can be partially or completely overlapped [3].

Vacuum ultraviolet (VUV) luminescence is one of the most powerful tools to study the low-temperature (10 K) spectroscopic properties of different kinds of phosphors containing varying amount of dopant [4]. Spectroscopic measurements under VUV excitation could be used to study radiative relaxation processes of electronic excitations, to specify the energy transfer mechanisms from host to activator, to identify the energy levels of dopant in the oxide host. Synchrotron radiation has been successfully applied to study relaxation processes of electronic excitation of different oxides in various crystalline forms, includingbulk crystals,

nanocrystals and thin films [5-6]. The differences reveled for the different crystalline forms of the same compound are related to variation of equilibrium defects concentration, which vary with fabrication method.

Rare-earth doped lutetium oxide is considered as an excellent optical material for phosphors, scintillators and solid-state lasers due to high melting point, hardness, chemical stability and good optical properties. It has isotropic cubic crystal structure, wide band gap of E_g=5.8-6,0 eV [7, 8], high solubility limits of rare-earth activator ions, low concentration quenching of luminescence due to low phonon energy. High density (ρ=9.44 g/cm^3), high X-ray stopping power, excellent radiation stability and high light yield of about 90000 photon/MeV [9] allow to consider Lu_2O_3:Eu^{3+}as effective scintillating material for X-ray radiography along with CsI:Tl, $CdWO_4$, $Bi_4Ge_3O_{12}$ crystals.

Preparation and luminescent properties and scintillation characteristics of Lu_2O_3:Eu^{3+} 5 at.% nanopowders and ceramics are widely studied (see, for example, [4, 8, 10-15]). Despite this fact, there is lack of information on luminescence properties of Lu_2O_3:Eu^{3+}transparent ceramics under VUV excitation. In [4] the low-temperature luminescence of Lu_2O_3:Eu^{3+}ceramics upon excitation with synchrotron radiation in the vicinity of band gap energy has been studied. It has been shown that the quite effective ways of host-to-activator energy transfer was revealed even at the very low temperature of 10 K, when the mobility of the carriers (especially holes) is very low. Multiplication of electronic excitations in Lu_2O_3:Eu^{3+}nanopowders with different size was studied in [8]. Impact excitation of Eu^{3+} ions by fast photoelectrons has been revealed. The energy transfer mechanisms from the host to Eu^{3+} ions have been determined. This work describes fabrication of Lu_2O_3:Eu^{3+} 5 at.% optical ceramics via vacuum sintering of co-precipitated nanopowders, as well as luminescence of Lu_2O_3:Eu^{3+} 5 at.% nanopowders and ceramics, excited by the VUV synchrotron radiation.

2 Experimental

2.1 Fabrication of Lu_2O_3:Eu^{3+}nanopowders and ceramics

$Lu_2O_3:Eu^{3+}$ 5 at.% (hereinafter referred to as $Lu_2O_3:Eu^{3+}$) nanocrystalline powder was obtained by normal-strike co-precipitation technique from water solution according to [16]. To produce optical ceramics,$Lu_2O_3:Eu^{3+}$nanopowders were pressed into disks by uniaxial pressing method at the pressure of 250 MPa. The relative density of compacts was 50% from the theoretical one. $Lu_2O_3:Eu^{3+}$compacts were sintered at T=1850°C in high vacuum (5×10^{-3} Pa) furnace with tungsten heaters and further annealed in air at T=1350°C for 15 h. Finally, the sintered ceramics were polished on both surfaces to the thickness of 1 mm.

2.2 Characterization of $Lu_2O_3:Eu^{3+}$nanopowders and ceramics

Morphology of the nanopowders was studied by transmission electronic microscopy (TEM-125, Selmi, Ukraine). Phase identification was performed by X-ray diffraction (XRD) method on a SIEMENS D-500 X-ray diffractometer (Cu_{Ka} radiation, graphite monochromator). Measurements of the optical transmittance of ceramics were conducted with 1 mm thick pellets polished on both surfaces. In-line transmittance in the 200-1100 nm wavelength range was determined using a Perkin-Elmer “LAMBDA-35” spectrophotometer. The luminescent properties of $Lu_2O_3:Eu^{3+}$nanopowder and ceramic samples were compared using the time-resolved luminescent spectroscopy under excitation by VUV synchrotron radiation (SR) with energy in the 3.7-25 eV range at the Superlumi station (DESY, Hamburg, Germany) at 8 K and 300 K. The emission/excitation spectra were registered in three time intervals: integral (1.2-100 ns), fast (1.2-20 ns) and slow (40-100 ns) after SR pulse with the duration of 0.126 ns.

3. Results and discussion

3.1Fabrication and optical properties of $Lu_2O_3:Eu^{3+}$ceramics

Fig. 1a shows the TEM image of $Lu_2O_3:Eu^{3+}$ nanocrystalline powders. The TEM image reveals that the crystallites are in the size range 20–50 nm. Fig. 1b shows the results of Rietveld refinement for a $Lu_2O_3:Eu^{3+}$nanopowders. According

to the XRD data, the nanopowders have cubic single phase with an average crystallite size of 33 nm and the lattice parameter a=10.4150 Å.

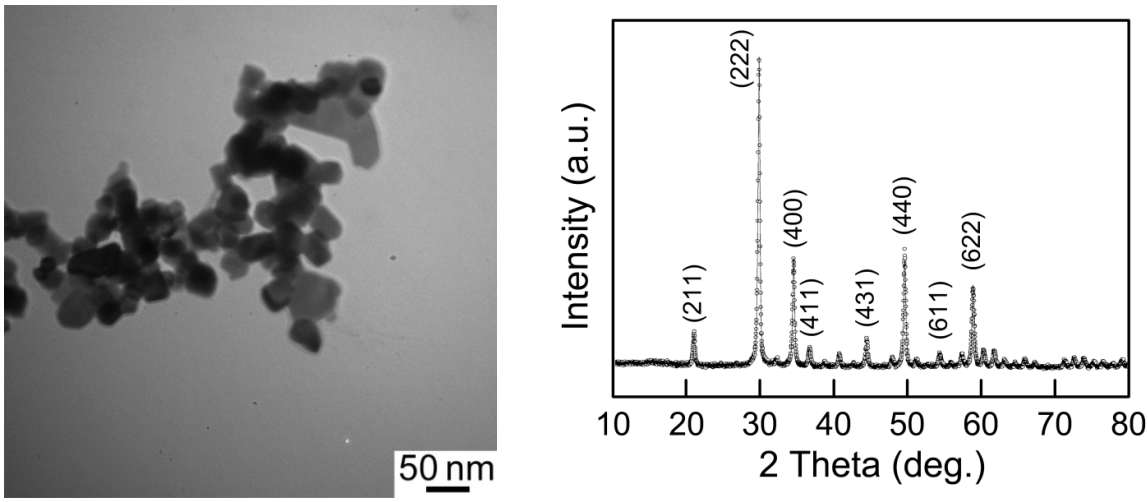

(a) (b)

Fig. 1 TEM image (a) and X-ray diffraction pattern (b) of Lu_2O_3:Eu^{3+}nanopowderscalcined at *T*=1000°C.

The vacuum sintering is considered as a perspective method for obtaining of transparent ceramics [17-18]. Relatively low driving force of densification, peculiar to this method, can be increased by using of special sintering aids that activate the consolidation processes [19]. Special attention should be addressed to choosing sintering aid in order to prevent degradation of optical transmittance of ceramics. As known, creation of secondary phases or defects in electronic subsystem, which act as charge carriers traps, results in degradation of optical properties of ceramics [20]. Densification rate of heteroionic compounds at the final sintering stage is controlled by the specimen with the lowest diffusion coefficient in the fastest diffusion path.

The diffusion coefficients of constituent elements in the lutetium oxide are unknown. At the same time, in the yttrium oxide, that is a structural analogue of Lu_2O_3, diffusion coefficients at 1600°C are 1.44×10^{-10} cm^2/s for Y^{3+} ions and 3.44×10^{-11} cm^2/s for O^{2-} ions [21]. Thus, the cations are diffusion-controlling specimen during sintering of the rare-earth oxides. It was shown recently [22] that europium ions capable of changing the valence stateare responsible not only for

scintillation response formation of Y_2O_3:Eu^{3+} ceramics, but also act as effective solid-state sintering aid. Doping of yttria by europium ions increases the effective diffusion constants by orders of magnitude due to controlling the defect chemistry onto cation sublattice [22]. Taking into account similar sintering mechanisms, one can expect that europium ions will play the same role in the structural analogue of Y_2O_3 – lutetium oxide.

We have compared optical properties of ceramics prepared from nominally pure and europium-doped Lu_2O_3nanopowders [14]. The europium concentration was chosen at 5 at%, which was close to the optimal activator concentration [23]. This composition is also optimal in terms of facilitating the sintering of Y_2O_3:Eu^{3+} isostructural ceramics [22]. ~~The powders were compacted using a uniaxial pressing method and sintered in vacuum at 1850°C for 15 hours.~~ Fig. 2 shows photos of Lu_2O_3 and Lu_2O_3:Eu^{3+}ceramics after vacuum sintering. The undoped ceramic samples were black and opaque (Fig. 2a), while the Lu_2O_3:Eu^{3+} ceramics, activated by the europium ions, were transparent and showed red emission under VUV excitation (Fig. 2b). The black color of ceramic is associated with the formation of oxygen-deficient lutetium oxide. A similar color was observed in RE_2O_3 (RE=Y, Lu) single crystals and ceramics obtained in a reducing environment [24]. Thus, the presence of activator ion significantly affects the optical transmittance of Lu_2O_3 ceramics (Fig. 2).

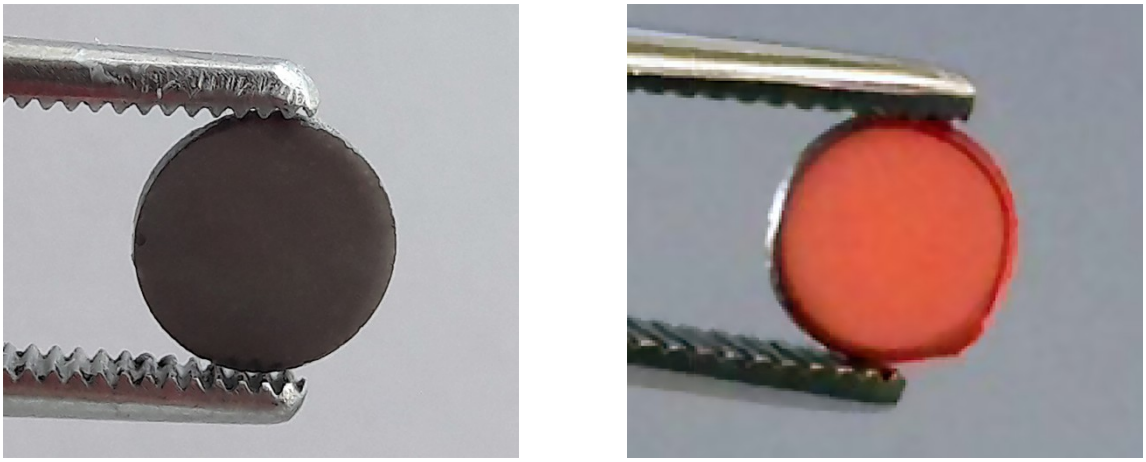

(a) (b)

Fig. 2. Photo of Lu_2O_3 (a) and Lu_2O_3:Eu^{3+}optical ceramics under UV excitation (b) after vacuum sintering at 1850°C for 15 h.

It is known that isovalent impurities practically do not affect the diffusion rate in compounds with fluorite-like structure [25]. Therefore, the intensification of the diffusion mass transfer in Lu_2O_3:Eu^{3+}ceramics could be associated with the change of the valence state of europium ions during vacuum sintering. In the starting Lu_2O_3:Eu^{3+}powder, the trivalent europium ions replace lutetium ions with the formation of a continuous series of Lu_2O_3:Eu^{3+}solid solutions. During the sintering process in environment with a strong reducing potential, the europium ions partially pass into a divalent state, since the electronic structure of Eu^{2+} is the most stable among all RE^{2+} cations. The compensation for the surplus charge occurs via formation of oxygen vacancies processing the lowest solution energy [26]:

$$2EuO + 2Lu_{Lu}^{X} + O_{O}^{X} \rightarrow 2Eu_{Lu}^{\square} + V_{O}^{\square} + Lu_2O_3 \quad (1)$$

The sintering mechanism of compounds with the sesquioxide crystal structure is limited by the diffusion of interstitial cations [25]. As shownabove, the valence change of the europium ions leads to the formation of the oxygen vacancies that compensate for excess charge. By analogy with Y_2O_3 [25], we can assume that increase the concentration of oxygen vacancies leads to an increase in the equilibrium concentration of interstitial lutetium ions. Obviously this result in amore effective densification of Lu_2O_3:Eu^{3+}ceramics. For example, for yttrium oxide doped by 5 at.% europium ions, effective diffusion coefficients increase by several orders of magnitude as compared to undoped material [22]. It is clear that in an isostructural lutetium oxide doping by 5 at% of europium ions leads to similar processes.

The activation of the diffusion mass transfer processes during the doping of lutetium oxide with europium ions is not only due to the change in the charge state of the activator ions, but also due to the local redistribution of electron density near the dopant [27-28]. The presence of dopant ions changes ionicity degree of Me–O chemical bond, which is manifested in the variation of bulk and grain boundary

diffusion coefficients. During reducing the effective charge of oxygen ions, the chemical bond becomes weaker, accompanying by an increase in atomic diffusion along the grain boundaries. Covalency degree of the RE–O chemical bonds in doped ceramics was estimated according to [28] taking into account the electronegativities of oxygen, lutetium and europium ions:

$$f_c=\exp(-\Delta\chi^2_p/4), \quad (2),$$

where χ_p is the difference in the electronegativity between cation and anion. χ_p for atoms relevant to this study are: $\chi(Lu^{3+})=1.431$, $\chi(Eu^{3+})=1.433$, $\chi(Eu^{2+})=1.181$, $\chi(O^{2-})=3.758$ [29]. Then the covalencies of the RE–O chemical bonds are equal to $f_c(Lu^{3+}–O)=0.258$, $f_c(Eu^{3+}–O)=0.259$, $f_c(Eu^{2+}–O)=0.190$. As can be seen, doping of lutetium oxide with trivalent europium ions does not change the covalency of chemical bonds. However, the transition of europium ions into the divalent state significantly reduces the strength of Eu–O chemical bonds [29]. It becomes more ionic, the density of the electronic cloud around the oxygen ions decreases, which contributes to the increase of diffusion mobility of atoms.

The in-line transmittance spectra of $Lu_2O_3:Eu^{3+}$ceramics before and after annealing in ambient atmosphereare shown in Fig. 3. Transmittance of undoped ceramics is not shown in Fig. 3, because it did not exceed 1%. Spectrum of $Lu_2O_3:Eu^{3+}$ceramics after vacuum sintering shows the characteristic absorption connected to $O^{2-}\rightarrow Eu^{3+}$ charge transfer transition (CTT) band in the 190-270 nm range and narrow lines in the 300-600 nm range, corresponding to 4f-4f transitions in Eu^{3+} ions. Moreover, wide absorption bands with maxima at 280 and 410 nm were observed[14]. These absorption bands are due to the formation of $2Eu^{\square}_{Lu}+V^{\square}_{O}$ complex defects. It is known that the bivalent europium ions [30] and F-like centers [31] can give additional absorption in this spectral range; therefore the revealing of the contribution from these defects is difficult. Similar broad absorption bands with close spectral position of the maxima were also attributed to the formation of bivalent europium ions in hot-pressed $Y_2O_3:Eu^{3+}$ ceramics [22].

The europium ions valence state and oxygen stoichiometry were recovered by air annealing of $Lu_2O_3:Eu^{3+}$ceramics (Fig. 3b). After heat treatment of ceramics the wide bands of additional absorption disappear, and the optical transmittance spectrum shows the characteristic features of trivalent europium ions in the lutetium oxide matrix. Annealing of $Lu_2O_3:Eu^{3+}$ceramics in air recovers oxygen vacancies and transfers europium ions to the trivalent charge state. The annealed $Lu_2O_3:Eu^{3+}$ceramics possess in-line optical transmittance of 50% in the 500-1100 nm wavelength range, which is about 60% of the theoretical value [32].

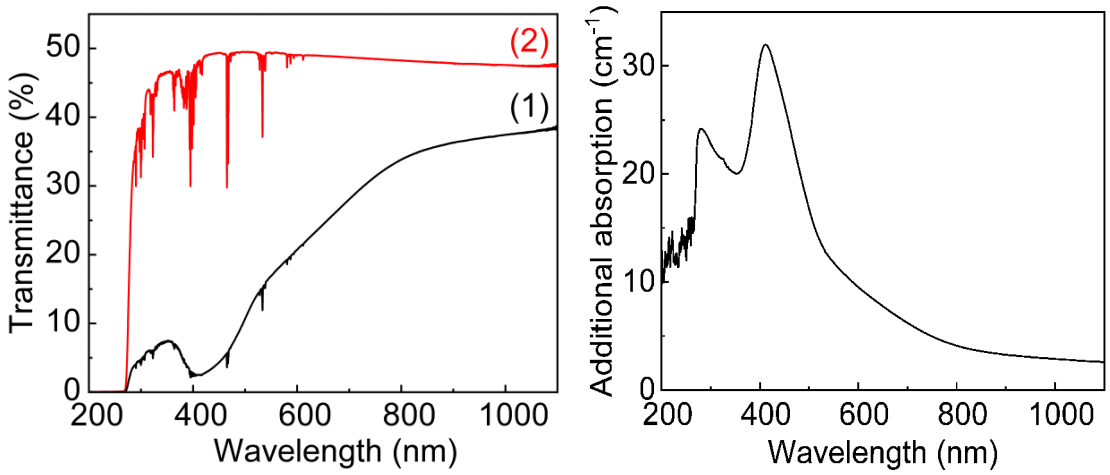

(a) (b)

Fig. 3. Transmittance of $Lu_2O_3:Eu^{3+}$ optical ceramics before (1) and after (2) annealing in air at 1350°C for 15 hours (a); additional absorption of defects in as-sintered $Lu_2O_3:Eu^{3+}$ optical ceramics (b).

3.2Luminescence properties of $Lu_2O_3:Eu^{3+}$nanopowders and ceramics

The luminescence spectra of $Lu_2O_3:Eu^{3+}$nanopowder and ceramic samples are quite different at the different energies of excitation at 8 K and 300 K (Fig. 4a and 4b). Generally, they consist of the group of lines caused by the $^5D_0 \rightarrow {}^7F_j$ transitions of Eu^{3+} ions. No emission of Eu^{2+} ions [33] was detected in all the $Lu_2O_3:Eu^{3+}$ samples under study. For $Lu_2O_3:Eu^{3+}$nanopowders, the most intensive peaks are observed at 610.8 nm and 609.7 nm at 8 K and 300 K, respectively. For $Lu_2O_3:Eu^{3+}$ ceramics, the position of most intensive peak is located at 609.6 nm at various

energies of excitation at 8 K and 300 K, except the excitation at 6.07 eV at 8K, when the main peak position is 611.7 nm.

It is well known that the structure of Lu_2O_3 lattice provides two positions with different symmetry for localization of Eu^{3+} ions; namely the centrosymmetric C_{3i} (S_6) and low-symmetric C_2 sites [8]. Therefore, the shifts of peak positions of Eu^{3+} luminescence in 609.6-609.7 nm and 610.8-611.7 nm ranges under excitation in the different points of the excitation spectra of Lu_2O_3:Eu nanopowder and ceramic can be caused by the $^5D_0 \rightarrow {}^7F_2$ transitions of Eu^{3+} ions in C_{3i} and C_2 positions, respectively.

It is also important to note here that luminescence light yield (LY) of the Lu_2O_3:Eu^{3+}nanopowders and ceramics, especially under high-energy excitation, strongly depends on the type and size of grain in these samples. The largest intensity is observed in ceramic sample, whereas in the case of nanopowders the LY is lower by a factor of 3 under the same conditions of excitation at 13.8-16.5 eV range. This is due to significant contribution of the surface states to the relaxation of high-energy excitation, especially for nanopowders. The surface of nanoparticles with large concentration of host defects is responsible for creation of so called “dead surface layer”, in which strong non-radiative losses of excitation energy on the host defects are observed [34]. This leads to decreasing the overall LY of the Eu^{3+} luminescence in Lu_2O_3:Eu^{3+}nanopowder.

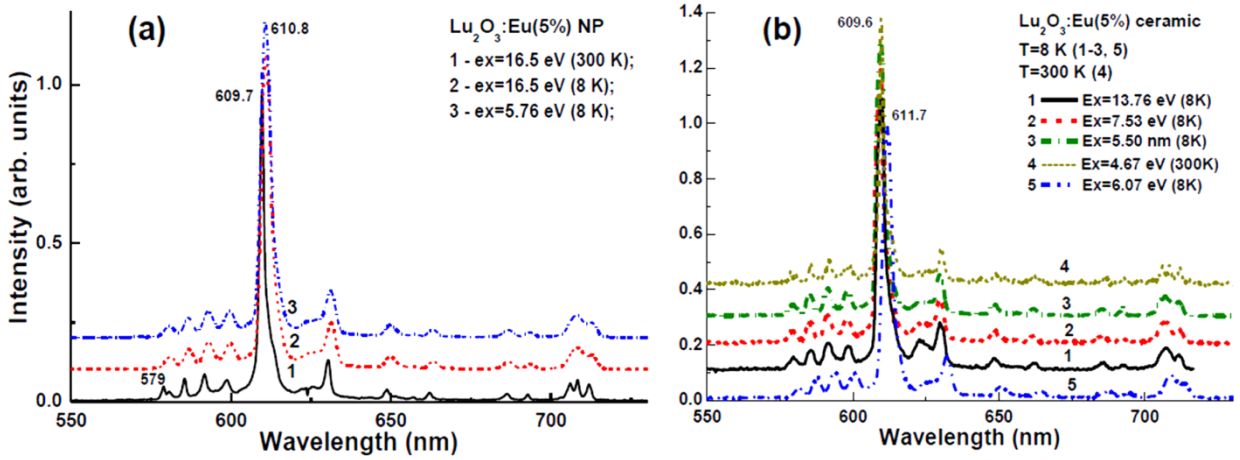

Fig. 4. Normalized emission spectra of Lu_2O_3:Eu^{3+}nanopowder (a) and ceramic (b) samples under excitation with the energy above the Lu_2O_3 band gap (1a, 2a, 1b, 2b); with energy close to the onset of interband transition (5b); with energy in the exciton range (3a, 3b) and with energy in the range of $O^{2-}\rightarrow Eu^{3+}$ CTT (4b) at 8 K (2a, 3a; 1a-3a, 5a) and 300 K (1a, 4b). For better presentation, spectra 2a and 3a in Fig. 4a and spectra 1b-4b in Fig. 4b were shifted by value of 0.1 along the Intensity axis.

The excitation spectra of the Eu^{3+} luminescence in the Lu_2O_3nanopowder (Fig. 5) and ceramic (Fig. 6) samples at 8 K and 300 K consist of the sharp lines in the 3.7-4.5 eV range, corresponding to the intrinsic 4f-4f ($^7F_{1,0}\rightarrow{}^5H_4$) transitions of Eu^{3+} ions. The wide bands peaked approximately at 5.0-4.885 eV in nanopowder and at 4.86-4.66 eV in ceramic samples are related to the $O^{2-}\rightarrow Eu^{3+}$ CTT. The bands, peaked at E_{ex}(Eu)=5.72-5.74 eV in nanopowder and at 5.62 eV in ceramic samples in the exciton range, correspond to energy of creation of the excitons bound with Eu^{3+} ions. Generally, the E_{ex}(Eu) value is a basic optical parameter of the materials; but in the case of large concentration of the host defects and strong participation of these defects in the excitation processes of impurity luminescence the position of this band typically is shifted to the low-energy side with respect to the peak corresponding for the creation of an exciton bound with the dopant in the unperturbed site. Taking into account this fact, the most high-energy peak at 5.74 eV is observed in the case of Lu_2O_3:Eu^{3+}nanopowders (Fig. 5a, curve 1), whereas in the case of ceramic sample the position of this peak is notably shifted to the low energy side to 5.62 eV (Fig. 6a, curve 1). Therefore, we can estimate that the E_{ex}(Eu) value in the Lu_2O_3:Eu^{3+} host is equal to 5.74 eV at 8 K. The bumps at 5.94 and 6.0 eV in the excitation spectra of Lu_2O_3:Eu^{3+}nanopowders and ceramics at 8 K, respectively, and at 5.8 eV in ceramic sample at 300 K most probably corresponds to the band gap value E_g of Lu_2O_3 host [8].

In the case of Lu_2O_3:Eu^{3+}nanopowders, the intensity of the luminescence substantially lower under excitation with the energy of Eu^{3+} CTT band and the band related to the creation of an exciton bound with Eu^{3+} ions in comparison with

Lu_2O_3ceramics (Figs. 6b and 7b, respectively). However, under excitation of the Lu_2O_3:Eu^{3+}nanopowders with the energies more than E_g value, the luminescence intensity of nanopowder sample significantly exceeds that for ceramic sample. Such effect is characteristic to the nanopowder samples with large dimension (above 60 nm), see [8] for details. The influence of nanopowder size on the recombination luminescence intensity is considered also in [35-36]. In the case of nanopowders with small size (a few nm), the electrons before recombination with activator centers, may be trapped by the surface defects or escape from nanopowders. The effects associated with spatial confinement should be included also along with the processes of resonance quenching by the surface impurities. These processes should lead to additional suppression of the luminescence as compared to the ceramics.

Taking into account the E_{ex}(Eu) and E_g values, we can also interpret in more detail the structure of the excitation spectra of Lu_2O_3:Eu^{3+}in the 8-25 eV range in terms of the multiplication of excitonic excitations[8, 15]. Namely, the observed several bands in the mentioned range can be related to the multiplication of corresponding excitation with the energies of nE_{ex}(Eu) and nE_g, where n=2, 3 and 4.

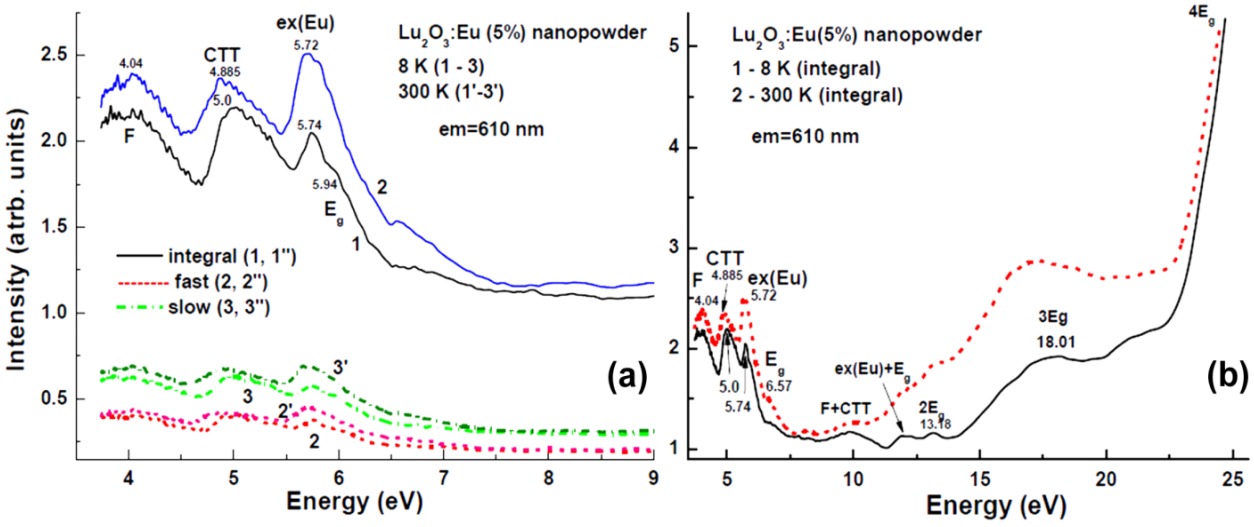

Fig. 5. Excitation spectra of integral (1, 1'), fast (2, 2') and slow (3, 3') components of Eu^{3+} luminescence at 610 nm in Lu_2O_3:Eu^{3+}nanopowders in 3.5-9 eV (a) and 3.5-26 eV (b) ranges at 8 K (1-3) and 300 K (1'-3').

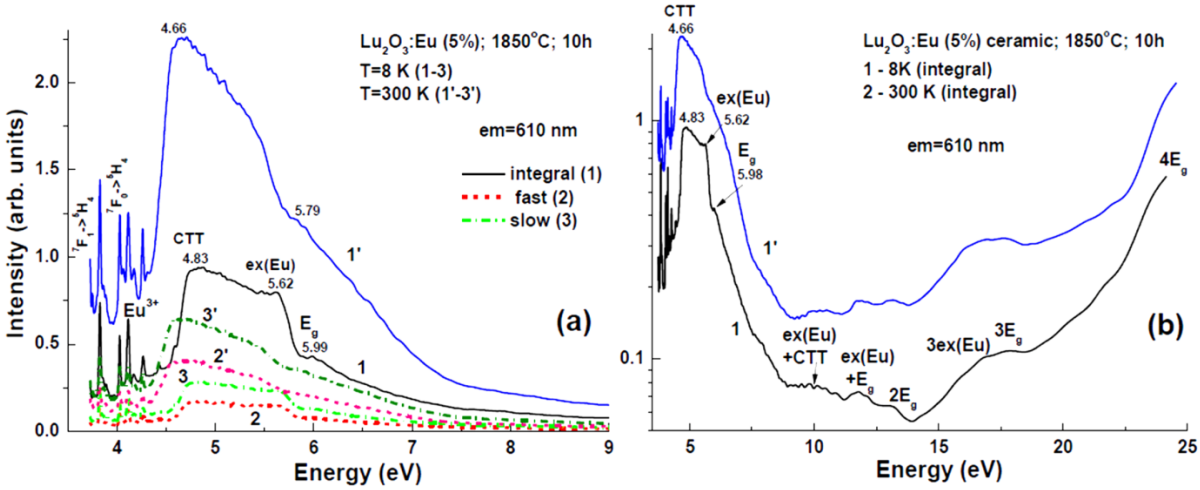

Fig. 6. Excitation spectra of integral (1, 1'), fast (2, 2') and slow (3, 3') components of Eu^{3+} luminescence at 610 nm in Lu_2O_3:Eu^{3+} ceramics in 3.5-9 eV (a) and 3.5-26 eV (b) ranges at 8 K (1-3) and 300 K (1'-3').

The characteristic feature of the excitation spectra of the Eu^{3+} luminescence in the Lu_2O_3:Eu^{3+}nanopowders (Fig. 5) consistsalso of the band peaked at 4.04 eV, related to the excitation of the Eu^{3+} emission via the F^+ centers luminescence (oxygen vacancies with one-trapped electrons) in the band peaked at 400 nm [15]. The emission band of F^+ centers is strongly overlapped with the most intensive Eu^{3+} excitation/absorption bands in this range, related to the $^7F_0 \rightarrow {}^5G_6$ and $^7F_0 \rightarrow {}^5L_6$ transitions. Taking into account that the oxygen vacancies and related with them F^+ centers in the large concentration are located mainly at the surface of nanopowders, we can presuppose also formation even the Eu^{3+}–F^+ pair centers in the surface layer of nanoparticles.

The energy level diagram of europium ions in Lu_2O_3:Eu^{3+}nanopowders and ceramics have been built using the result of luminescence measurements (Fig. 7). E_g, $O^{2-} \rightarrow Eu^{2+}$ CTT band and the band related to the creation of an exciton bound with Eu^{3+} ions are labeled in the Fig. 7. Moreover, the energy level positions of Eu^{2+} ions in the band gap of Lu_2O_3 ceramics and nanopowders have been also determined using approach proposed in [37]. Dorenbos suggests [37] that the position of $O^{2-} \rightarrow Eu^{2+}$ CTT band allows one to establish the ground state position of Eu^{2+} ions relative to the valence band. Since the energies of the first $4f^7 \rightarrow 4f^6 5d$ transitions of Eu^{2+} ions in Lu_2O_3 are unknown, the energy of observed Eu^{2+} transitions in other

oxides were labeled on the scheme (E=1.43–3.50eV) [30]. This model predicts that luminescence of Eu^{2+} in lutetium oxide is totally quenched. The estimation and experimental observation gives Lu_2O_3 band gap width value of $E_g \approx 5.95$ eV [15, 31]. So the excited levels of the Eu^{2+} ions in Lu_2O_3 are located in the conduction band for both nanopowders and ceramics (Fig. 7).

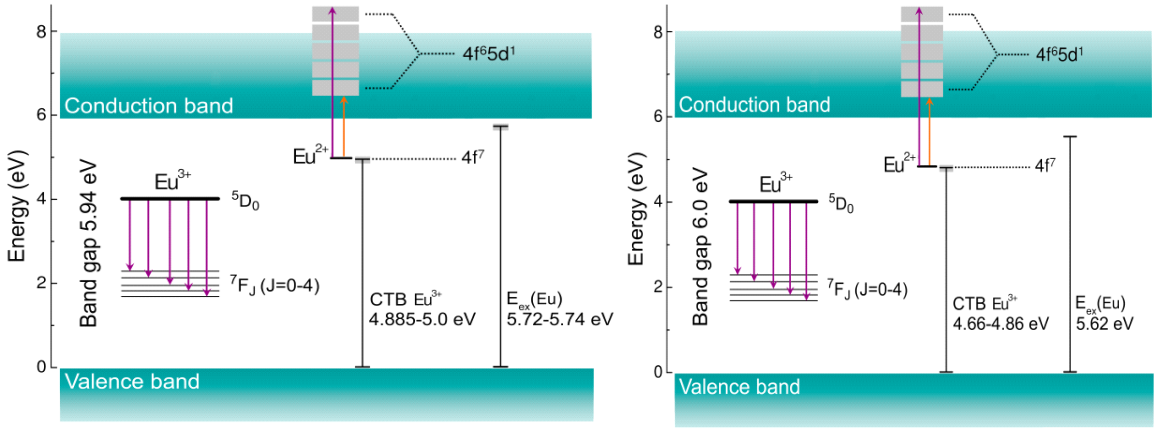

(a) (b)

Fig 7. Energy level diagram of europium ions in Lu_2O_3:Eu^{3+}nanopowders (a) and ceramics (b).

4. Conclusions

Lu_2O_3:Eu^{3+} 5 at.% nanopowders were produced by co-precipitation method, while Lu_2O_3:Eu^{3+} transparent ceramics with in-line optical transmittance of 50% in the visible wavelength range were fabricated by vacuum sintering. It was determined that transition of a part of europium ions into divalent state significantly changed the diffusion mass transfer due to formation of anionic vacancies and decreasing the covalency of RE–O bonds in the doped material.

The luminescent properties of Lu_2O_3:Eu^{3+}nanopowders and transparent ceramics were studied at 8 and 300 K using synchrotron radiation excitation in the 3.7-25 eV range. It was found that the notable differences in the excitation spectra of Lu_2O_3:Eu^{3+}nanopowders and ceramics were caused by participation of the F^+ centers located at the surface of nanopowders in the excitation processes of Eu^{3+} luminescence in Lu_2O_3 host. The positions of the energy levels related to the Eu^{3+}

dopant in Lu_2O_3matrix were determined more exactly. The energy of creation of excitons bound with the Eu^{3+} in the Lu_2O_3:Eu^{3+} and energy band gap of Lu_2O_3 were estimated to be 5.7 eV and 6.0 eV at 8 K. We also observed the differences in energies of creation of excitons bound with the Eu^{3+} ions in Lu_2O_3:Eu^{3+}nanopowdersand ceramics. They were caused by participation of the host defects and impurities in the excitation processes of Eu^{3+} luminescence.

Acknowledgments

Authors are grateful to Dr. O.M. Vovk for his help in characterization of experimental samples. This work was partially supported by the National Academy of Sciences of Ukraine within the frame of the project “Nanoceramics”, as well as by the Polish NCN 2016/21/B/ST8/03200 project. The investigations at Superlumi station were performed within I-20110938 EC project.

References

[1] V. Mürk, B. Namozov, N. Yaroshevich, Complex oxides: Electron excitations and their relaxation, Radiat. Meas. 24 (1995) 371-374. https://doi.org/10.1016/1350-4487(95)00017-9.

[2] V. Murk, N. Yaroshevich, Exciton and recombination processes in YAG crystals, J. Phys. Condens. Matter. 7 (1995) 5857–5864. https://doi.org/10.1088/0953-8984/7/29/012.

[3] I. N. Ogorodnikov, V. A. Pustovarov, M. Kirm, A. V. Kruzhalov, L. I. Isaenko,Electron excitations in LiB_3O_5crystals with defects: Low-temperature time-resolved luminescence VUV spectroscopy, Phys. Solid State 43 (2001)1454–1463. https://doi.org/10.1134/1.1395083.

[4] E. Zych, J. Trojan-Piegza, Low-temperature luminescence of Lu_2O_3:Eu ceramics upon excitation with synchrotron radiation in the vicinity of band gap energy, Chem. Mater. 18 (2006) 2194–2199. https://doi.org/10.1021/cm052774q.

[5] T. Zorenko, V. Gorbenko, A, Petrosyan, W. Gieszczyk, P. Bilski, Y. Zorenko, Intrinsic and defect-related luminescence of $YAlO_3$ and $LuAlO_3$ single crystals and films, Opt. Mater. 86 (2018) 376–381. https://doi.org/10.1016/j.optmat.2018.10.029.

[6] V. Gorbenko, E. Zych, T. Voznyak, S. Nizankovskiy, T.Zorenko, Y. Zorenko, Comparison of the luminescent properties of LuAG:Prnanopowders, crystals and films using synchrotron radiation, Opt. Mater. 66 (2017) 271–276.https://doi.org/10.1016/j.optmat.2017.02.003.

[7] Hong Jiang, Patrick Rinke, and Matthias Scheffler, Electronic properties of lanthanide oxides from the GW perspective, Phys. Rev. B 86 (2012) 125115-1-13. https://doi.org/10.1103/PhysRevB.86.125115.

[8] V. Makhov, C. Lushchik, A. Lushchik, M. Kirm, Z.F. Wang, W.P. Zhang, M. Yin, J.T. Zhao, Multiplication of electronic excitations in nanophosphors $Lu_2O_3:Eu^{3+}$ and $Lu_2O_3:Tb^{3+}$, J. Lumin. 129 (2009) 1711–1714. https://doi.org/10.1016/j.jlumin.2008.12.028.

[9] Y. Shi, Q.W. Chen, J.L. Shi, Processing and scintillation properties of Eu^{3+} doped Lu_2O_3 transparent ceramics, Opt. Mater. 31 (2009) 729–733. https://doi.org/10.1016/j.optmat.2008.04.017.

[10] J. Sanghera, W. Kim, C. Baker, G. Villalobos, J. Frantz, B. Shaw, A. Lutz, B. Sadowski, R. Miklos, M. Hunt, F. Kung, I. Aggarwal, Laser oscillation in hot pressed 10% $Yb^{3+}:Lu_2O_3$ ceramic, Opt. Mater. 33 (2011) 670–674. https://doi.org/10.1016/j.optmat.2010.09.012.

[11] Z. M. Seeley, J. D. Kuntz, N. J. Cherepy, S. A. Payne, Transparent Lu_2O_3:Eu ceramics by sinter and HIP optimization, Opt. Mater. 33 (2011) 1721–1726. https://doi.org/10.1016/j.optmat.2011.05.031.

[12] L. An, A. Ito, T. Goto, Fabrication of transparent lutetium oxide by spark plasma sintering, J. Amer. Ceram. Soc. 94 (2011) 695–698. https://doi.org/10.1111/j.1551-2916.2010.04145.x.

[13] R. Boulesteix, R. Epherre, S. Noyau, M. Vandenhende, A. Maitre, C. Sallé , G. Alombert-Goget, Y. Guyot, A. Brenier, Highly transparent Nd:Lu_2O_3

ceramics obtained by coupling slip-casting and spark plasma sintering, Scripta Materialia 75 (2014) 54–57. https://doi.org/10.1016/j.scriptamat.2013.11.016.

[14] Yu.L. Kopylov, V.B. Kravchenko, N.A. Dulina, A.V. Lopin, S.V. Parkhomenko, A.V. Tolmachev, R.P. Yavetskiy, O.V. Zelenskaya Fabrication and characterization of Eu^{3+}-doped Lu_2O_3 scintillation ceramics Opt. Mater. 35 (2013) 812–816. https://doi.org/10.1016/j.optmat.2012.04.020.

[15] T. Zorenko, V. Gorbenko, N. Dulina, N. Matveevskaya, R. Yavetskiy, N. Babayevskaya, Yu. Zorenko, Comparative study of the luminescent properties of oxide compounds under synchrotron radiation excitation: Lu_2O_3:Eu nanopowders, ceramics and films, J. Lumin., 199 (2018) 461–464. https://doi.org/10.1016/j.jlumin.2018.03.044.

[16] N.A. Dulina, V.N. Baumer, M.I. Danylenko, P.V. Mateychenko, A.V. Tolmachev, O.M. Vovk, R.P. Yavetskiy, Effects of phase and chemical composition of precursor on structural and morphological properties of $(Lu_{0.95}Eu_{0.05})_2O_3$ nanopowders, Ceram. Int. 39 (2013) 2397–2404. https://doi.org/10.1016/j.ceramint.2012.08.092.

[17] W. Xie, J. Wang, M. Cao, Z. Hu, Y. Feng, X. Chen, N. Jiang, J. Dai, Y. Shi, V. Babin, E. Mihóková, M. Nikl, J. Li, Fabrication and properties of Eu:Lu_2O_3 transparent ceramics for X-ray radiation detectors, Opt. Mater. 80 (2018) 22–29. https://doi.org/10.1016/j.optmat.2018.04.029.

[18] W.-F. Xie, J. Wang, M. Ivanov, R. Yavetskiy, N. Jiang, Y. Shi, H.-H. Chen, H. Kou, J. Li, Eu:Lu_2O_3 transparent ceramics fabricated by vacuum sintering of co-precipitated nanopowders, Opt. Mater. 86 (2018) 550–561. https://doi.org/10.1016/j.optmat.2018.10.055

[19] X. Zou, H. Yi, G. Zhou, S. Chen, Y. Yang, S. Wang, Highly transmitting ZrO_2-doped Lu_2O_3 ceramics from combustion synthesized powders, J. Am. Ceram. Soc. 94 (2011) 2772–2774. https://doi.org/10.1111/j.1551-2916.2011.04710.x.

[20] C.G. Levi, Metastability and microstructure evolution in the synthesis of inorganics from precursors, Acta Mater. 46 (1998) 787–800. https://doi.org/10.1016/S1359-6454(97)00260-7.

[21] G. Bernard-Granger, C. Guizard, L. San-Miguel, Sintering behavior and optical properties of yttria, J. Am. Ceram. Soc. 90 (2007) 2698–2702. https://doi.org/10.1111/j.1551-2916.2007.01759.x.

[22] S.R. Podowitz, R. Gaumé, R.S. Feigelson, Effect of europium concentration on densification of transparent Eu:Y_2O_3 scintillator ceramics using hot pressing, J. Am. Ceram. Soc. 93 (2010) 82–88. https://doi.org/10.1111/j.1551-2916.2009.03350.x.

[23] A. Lempicki, C. Brecher, P. Szupryczynski, H. Lingertat, V.V Nagarkar, S.V. Tipnis, S.R. Miller, A new lutetia-based ceramic scintillator for X-ray imaging, Nucl. Instruments Methods Phys. Res. Sect. A Accel. Spectrometers, Detect. Assoc. Equip., 488 (2002) 579–590. https://doi.org/10.1016/S0168-9002(02)00556-9.

[24] Y. Tsukuda, Properties of black Y_2O_3 sintered bodies, Mater. Res. Bull. 16 (1981) 453–459. https://doi.org/10.1016/0025-5408(81)90013-1.

[25] P.-L. Chen, I.-W. Chen, Grain boundary mobility in Y_2O_3: Defect mechanism and dopant effects, J. Am. Ceram. Soc. 79 (1996) 1801–1809. https://doi.org/10.1111/j.1151-2916.1996.tb07998.x.

[26] M. R. Levy, C. R. Stanek, A. Chroneos, R. W. Grimes, Defect chemistry of doped bixbyite oxides, Solid State Sci. 9 (2007) 588–593. https://doi.org/10.1016/j.solidstatesciences.2007.02.009.

[27] M. Kodo, K. Soga, H. Yoshida, T. Yamamoto, Doping effect of divalent cations on sintering of polycrystalline yttria, J. Eur. Ceram. Soc. 30 (2010) 2741–2747. https://doi.org/10.1016/j.jeurceramsoc.2010.05.028.

[28] K. Ohgushi, J. Yamaura, M. Ichihara, Y. Kiuchi, T. Tayama, T. Sakakibara, H. Gotou, T. Yagi, Y. Ueda, Structural and electronic properties of pyrochlore-type $A_2Re_2O_7$ (A=Ca, Cd, and Pb), Phys. Rev. B 83 (2011) 125103. https://doi.org/10.1103/PhysRevB.83.125103.

[29] K. Li, D. Xue. Estimation of electronegativity values of elements in different Valence States, J. Phys. Chem. A 110 (2006) 11332–11337. https://doi.org/10.1021/jp062886k.

[30] P. Dorenbos, Energy of the first $4f^7 \rightarrow 4f^6 5d$ transition of Eu^{2+} in inorganic compounds, J. Lumin. 104 (2003) 239–260. https://doi.org/10.1016/S0022-2313(03)00078-4.

[31] A.I. Popov, E.A. Kotomin, J. Maier, Basic properties of the F-type centers in halides, oxides and perovskites, Nucl. Instruments Methods Phys. Res. Sect. B Beam Interact. with Mater. Atoms, 268 (2010) 3084–3089. https://doi.org/10.1016/j.nimb.2010.05.053.

[32] A.A. Kaminskii, M.S. Akchurin, P. Becker, K. Ueda, L. Bohatý, A. Shirakawa, M. Takurakawa, K. Takaichi, H. Yagi, J. Dong, T. Yanagitani, Mechanical and optical properties of Lu_2O_3 host-ceramics for Ln^{3+} lasants, Laser Phys. Lett. 5 (2007) 300–303. https://doi.org/10.1002/lapl.200710128.

[33] G. Bellocchi, G. Franzò, F. Iacona, S. Boninelli, M. Miritello, T. Cesca, F. Priolo, Eu^{3+} reduction and efficient light emission in Eu_2O_3 films deposited on Si substrates, Optics Express 20 (2012) 5501–5507. https://doi.org/10.1364/OE.20.005501.

[34] N.V. Babayevskaya, A.S. Bezkrovnyi, P.V. Mateychenko, O.M. Vovk, R.P. Yavetskiy, Sol-gel processing of transparent Lu_2O_3:Eu^{3+} phosphor films, Funct. Mater. 17 (2010) 537–542.

[35] V.V. Vistovskyy, A.V. Zhyshkovych, N.E. Mitina, A.S. Zaichenko, A.V. Gektin, A.N. Vasil'ev, A.S. Voloshinovskii. Relaxation of electronic excitations in CaF_2 nanoparticles, J. Appl. Phys. 112 (2012) 024325. https://doi.org/10.1063/1.4739488.

[36] T.S. Malyy, V.V. Vistovskyy, Z.A. Khapko, A.S. Pushak, N.E. Mitina, A.S. Zaichenko, A.V. Gektin, A.S. Voloshinovskii. Recombination luminescence of $LaPO_4$-Eu and $LaPO_4$-Pr nanoparticles J. Appl. Phys. 113 (2013) 224305. https://doi.org/10.1063/1.4808797.

[37] P. Dorenbos, Systematic behaviour in trivalent lanthanide charge transfer energies, J. Phys. Condens. Matter. 15 (2003) 8417–8434. https://doi.org/10.1088/0953-8984/15/49/018.

Figure captions

Fig. 1 TEM image (a) and X-ray diffraction pattern (b) of $Lu_2O_3:Eu^{3+}$ nanopowders calcined at *T*=1000°C.

Fig. 2. Photo of Lu_2O_3 (a) and $Lu_2O_3:Eu^{3+}$ optical ceramics under UV excitation (b) after vacuum sintering at 1850°C for 15 h.

Fig. 3. Transmittance of $Lu_2O_3:Eu^{3+}$ optical ceramics before (1) and after (2) annealing in air at 1350°C for 15 hours (a); additional absorption of defects in as-sintered $Lu_2O_3:Eu^{3+}$ optical ceramics (b).

Fig. 4. Normalized emission spectra of $Lu_2O_3:Eu^{3+}$nanopowder (a) and ceramic (b) samples under excitation with the energy above the Lu_2O_3 band gap (1a, 2a, 1b, 2b); with energy close to the onset of interband transition (5b); with energy in the exciton range (3a, 3b) and with energy in the range of $O^{2-}\rightarrow Eu^{3+}$ CTT (4b) at 8 K (2a, 3a; 1a-3a, 5a) and 300 K (1a, 4b). For better presentation, spectra 2a and 3a in Fig. 4a and spectra 1b-4b in Fig. 4b were shifted by value of 0.1 along the Intensity axis.

Fig. 5. Excitation spectra of integral (1, 1”), fast (2, 2”) and slow (3, 3’) components of Eu^{3+} luminescence at 610 nm in $Lu_2O_3:Eu^{3+}$ nanopowders in 3.5-9 eV (a) and 3.5-26 eV (b) ranges at 8 K (1-3) and 300 K (1’-3’).

Fig. 6. Excitation spectra of integral (1, 1”), fast (2, 2”) and slow (3, 3’) components of Eu^{3+} luminescence at 610 nm in $Lu_2O_3:Eu^{3+}$ ceramics in 3.5-9 eV (a) and 3.5-26 eV (b) ranges at 8 K (1-3) and 300 K (1’-3’).

Fig 7. Energy level diagram of europium ions in $Lu_2O_3:Eu^{3+}$ nanopowders (a) and ceramics (b).